Epidural Spinal Cord Stimulation: Calculation of Field Potentials with Special Reference to Dorsal Column Nerve Fibers

Johannes J. Struijk, *Student Member, IEEE,* Jan Holsheimer, Benno K. van Veen, and Herman B. K. Boom, *Member, IEEE*

Abstract—**The effect of electrical stimulation with several electrode combinations on nerve fibers with different orientations in the spinal cord was investigated by computing the steady-state field potentials and activating functions. At first an infinite homogeneous model was used while secondly the spinal cord and its surrounding tissues were modeled as an inhomogeneous anisotropic volume conductor. The effect of mediodorsal epidural stimulation was calculated. It was concluded that with cathodal stimulation, mediodorsally in the epidural space, longitudinal fibers are depolarized, but dorsoventral ones are hyperpolarized. With anodal stimulation the opposite will occur. It was found that parameters substantially affecting the potential distribution in the dorsal columns are the conductivity of the white matter and the width and the conductivity of the csf layer.**

Introduction

In 1967 Shealy [1] was the first who treated a patient, suffering from chronic pain, with epidural spinal cord stimulation (SCS). A good analgesic effect was obtained from this stimulation. Up to now SCS has been used with thousands of patients with various diseases, such as chronic pain, spasticity, peripheral vascular disease, bladder dysfunction, torticollis, etc., with varying results.

Yet SCS is poorly understood. Except for the treatment of chronic pain which initially was based on the "gate control" theory of Melzack and Wall [2], [3], there are no adequate explanations of the neurophysiological effects of SCS, although numerous hypotheses of the underlying neurophysiological mechanisms exist [4]. This lack of knowledge is a serious difficulty in attempts to improve SCS results and thus little progress has been made in the last decade. It is unknown which parts of the spinal cord have to be stimulated to obtain maximum benefit and despite more than 20 years of SCS practice, there is no agreement on the optimal values of stimulation parameters such as frequency, electrode position and configuration, pulse duration, etc., in the treatment of various disorders.

Potential distributions in the spinal cord due to stimulation are not well known. These potential distributions were measured in cadaver spinal cord by Swiontek *et al.* [5] and calculated using a two-dimensional computer model by Rusinko *et al.* [6] and Coburn and Sin [7], [8]. Because, for point-like sources, 3-D solutions of the field problem are essentially different from 2-D solutions, two-dimensional calculations have a restricted value. A three-dimensional analysis was therefore made by Coburn and Sin [9] with a bipolar electrode configuration using point sources. The influence of parameter variability was investigated by Coburn and Sin in the 2-D model but not in the 3-D model.

In order to investigate which parts of the spinal cord will be stimulated in "standard" epidural spinal cord stimulation and how this stimulation will be influenced by anatomical variability and electrode configuration, the 3-D steady-state potential field was calculated in an infinite homogeneous medium, and in a more realistic inhomogeneous anisotropic model of the spinal cord. The effect on spinal nerve fibers was approximated using the activating function [10] which, for myelinated fibers, is the second order difference of the extracellular potentials along the fiber. According to the model of McNeal [11] a positive value of the activating function corresponding to membrane depolarization and a negative one to hyperpolarization as was shown by Rattay [10]. The activating function can be approximated by the second derivative ("continuous activating function") at larger distances between fiber and electrode [12], as in epidural SCS.

Anatomy

The spinal cord is situated in the spinal canal which is enclosed by the vertebral processes and the dorsal side of the vertebrae. The transverse section of the spinal cord is more or less circular, but varies with the segmental level.

In Fig. 1 a transverse section of the spinal cord and surrounding tissues is shown. Within the spinal canal the spinal cord is surrounded by the cerebrospinal fluid (csf), which is enclosed by membranes. The inner membrane, or pia mater, encloses the spinal cord. The pia is connected by thin filaments to the arachnoid which, in turn, is surrounded by the dura mater. The epidural space between dura and vertebral bone consists of epidural fat and bloodvessels. The spinal cord itself is composed of white and gray matter. White matter consists of myelinated nerve fibers and gray matter is composed of cell bodies with their dendritic trees and small unmyelinated fibers. A comprehensive description of the anatomy and physiology of the spinal cord is given by Davidoff [13].

In mediodorsal epidural stimulation it is mainly the dorsal column fibers that will be stimulated. These (primary sensory) fibers enter the spinal cord by the dorsal roots and then enter the gray matter or continue towards the dorsal columns where they split up into an ascending branch to higher spinal and supraspinal levels and into a descending branch to lower levels.

Manuscript received June 8, 1989; revised February 28, 1990. This work was supported by the Dutch Innovative Research Program on Aids for the Handicapped (IOP-HG).

The authors are with the Biomedical Engineering Division, Department of Electrical Engineering, University of Twente, 7500 AE Enschede, The Netherlands.

IEEE Log Number 9042384.

0018-9294/91/0100-0104$01.00 © 1991 IEEE

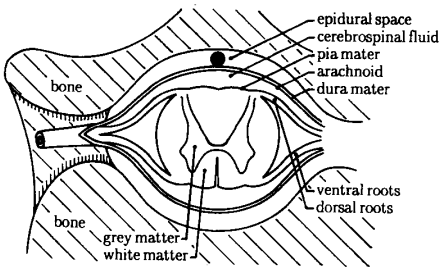

Fig. 1. Transverse section of the spinal cord and its surrounding tissues.

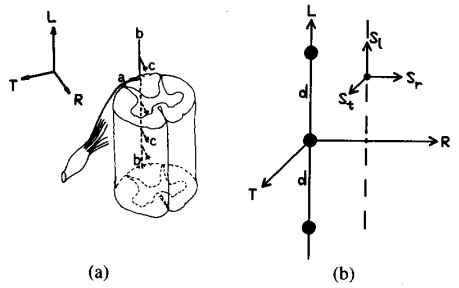

Fig. 2. (a) Sensory fibers in the dorsal columns. *a*—Primary afferent entering the dorsal columns, *b*—longitudinal ascending and descending branches and *c*—collaterals. (b) Definition of activating functions in longitudinal (S_l), tangential (S_t) and radial (S_r) directions. The electrode array is located at the *L*-axis and the electrodes are separated by a distance *d*.

At both higher and lower levels these fibers have dorsoventral collaterals as shown in Fig. 2(a). Thus, as seen from an epidural electrode in the midsagittal plane, different parts of the sensory fibers have almost perpendicular orientations. In the coordinate system shown in Fig. 2(b) [with reference to Fig. 2(a)] ascending and descending fibers (*b*) have a longitudinal orientation, the continuations of the dorsal root fibers (*a*) have a tangential orientation and the collateral branches (*c*) have a radial one.

Model Description

In order to calculate the potential distribution in the spinal cord a volume conductor model was used that, although simplified, takes into account the major geometrical characteristics. The space of interest is divided into identical wedge-shaped volume elements. In a longitudinal direction the model is composed of 40 layers, each consisting of 3000 volume elements, orderly arranged in rows of 61–99 wedges. These wedges appear as equilateral triangles in every transverse section of the model. Each volume element was given an (an)isotropic conductivity.

As shown in Fig. 6(a) the model comprises gray matter, white matter, cerebrospinal fluid, epidural fat and a low conductivity layer around the epidural space. This layer represents the peripheral parts, like the vertebral bone, muscle, fat, and skin. In Table I the conductivities of these compartments are summarized. Values are taken from Geddes and Baker [14], except for the conductivity of csf, which we measured in samples from three subjects at a temperature of 37°C and a frequency of 1 kHz.

Dura mater, pia mater, and arachnoid were not incorporated in the model. Sin and Coburn [8] estimated that these membranes will only negligibly influence the field potential distribution in the spinal cord.

TABLE I
Conductivities of the Compartments in the Inhomogeneous Anisotropic Model

Compartment	Conductivity $(\Omega \cdot \text{cm})^{-1}$
gray matter (gm)	0.0023
white matter (wm)	0.0060 longitudinal 0.00083 transversal
cerebro sp fl (csf)	0.017
epidural fat (ef)	0.00040
surrounding layer	0.00002

TABLE II
Sagittal Diameters of the Spinal Cord and the Subarachnoid Space at Level C5 and C6 (in mm)

	Spinal Cord		Subarachnoid Space	
	C5	C6	C5	C6
Elliott [15]	7.7		13.2	
Nordquist [16]	9.5	9.1		
Di Chiro	8.5		14	
Penning [17]	7.1		13.8	
Thyssen [18]	6.2	6.4	11.8	10.5
Skalpe [19]	7.0	7.0		

Some geometrical parameters of the compartments are poorly known or variable. Especially the width of the subarachnoid space at cervical levels is variable, because it depends on the set of the head. Data in literature on normal subjects are inconsistent (Table II). This is partly due to the different radiological methods that were used. The average sagittal diameter of the spinal cord at level C5/C6 in normal subjects ranges from 6.2 to 9.5 mm. In the model an average value of 7.4 mm was used. The coronal diameter of the spinal cord was taken to be 12.6 mm, thus being in agreement with the sagittal/coronal ratio that was estimated from photographs of transverse sections of the spinal cord at level C5/C6. The width of the csf layer was taken to be 1.4 mm. This is rather arbitrary because the width is very variable. The length of the model was 60 mm.

Computational Method

Homogeneous Model

As a first approximation of the influence of different electrode configurations on distant nerve fibers having different orientations, the activating functions in a homogeneous medium were calculated analytically in three orthogonal directions [Fig. 2(b)]. With point sources in $(R, T, L) = (0, 0, L_i)$ the field potential φ can be written as

$$\varphi(R, T, L) = \frac{1}{4\pi\sigma} \sum_{i=1}^{N} \frac{I_i}{\left[R^2 + T^2 + (L - L_i)^2\right]^{1/2}}$$

where I_i is the current of point source i and R, T, L the coordinates as defined in Fig. 2(b).

Differentiating φ twice in the related direction yields the (continuous) activating functions in a longitudinal ($S_L = \partial^2\varphi/\partial L^2$), radial ($S_R = \partial^2\varphi/\partial R^2$) and tangential ($S_T = \partial^2\varphi/\partial T^2$) direction:

							+1/2	−1/2	+1/2
		+1/2	−1/2	+1	−1/2	+1/2	−1/2	+1/2	−1/2
+1	−1	+1/2	−1/2	−1	+1	−1	−1/2	+1/2	+1/2
					−1/2	+1/2	+1/2	−1/2	−1/2
a	c	aa	cc	ac	cac	aca	acca	caac	acac

Fig. 3. Configurations of a four electrode array. a = anode, c = cathode. With configurations a, c, aa, and cc a distant reference electrode is assumed.

$$S_L(R, T, L) = -\frac{1}{4\pi\sigma}\sum_{i=1}^{N} I_i \frac{R^2 + T^2 - 2(L - L_i)^2}{\left[R^2 + T^2 + (L - L_i)^2\right]^{5/2}} \tag{1a}$$

$$S_R(R, T, L) = -\frac{1}{4\pi\sigma}\sum_{i=1}^{N} I_i \frac{-2R^2 + T^2 + (L - L_i)^2}{\left[R^2 + T^2 + (L - L_i)^2\right]^{5/2}} \tag{1b}$$

$$S_T(R, T, L) = -\frac{1}{4\pi\sigma}\sum_{i=1}^{N} I_i \frac{R^2 - 2T^2 + (L - L_i)^2}{\left[R^2 + T^2 + (L - L_i)^2\right]^{5/2}}. \tag{1c}$$

The electrodes are at equidistant positions [intervals d in Fig. 2(b)]. Activating functions in the three orthogonal directions were calculated for different configurations of an array of one to four electrodes, as commonly used (Fig. 3).

Inhomogeneous Model

Instead of solving Laplace's equation for calculating field potentials in the inhomogeneous model, a variational principle was used: a functional representing the power dissipation of the potential field must be minimized to obtain the solution [40], [41]. Applying this method, inhomogeneities, anisotropy, and different boundary conditions can easily be incorporated and only first order derivatives are used while in direct discretization methods (of Laplace's equation) second-order derivatives appear. In case no current source is present the power dissipation functional is given by

$$P(\varphi) = \iiint_V \tfrac{1}{2}\,\bar{\nabla}\varphi \cdot \bar{\bar{\sigma}}\,\bar{\nabla}\varphi\, dV \tag{2}$$

where φ is the field potential, $\bar{\bar{\sigma}}$ is the conductivity tensor (only the diagonal elements are non-zero), V is the volume of the model. The boundary conditions are of Dirichlet type

$$\varphi = \text{constant at the electrode surface} \tag{3a}$$

$$\varphi = 0 \text{ at the model surface.} \tag{3b}$$

The power dissipation P_w in one wedge can be calculated according to (2) using coordinates ξ, η, ζ (Fig. 4):

$$P_w(\varphi) = \frac{1}{\sqrt{3}}\int_{\zeta=0}^{k}\int_{\eta=0}^{h-\xi}\int_{\xi=0}^{h}\left\{\sigma_x\left(\frac{\partial\varphi}{\partial\xi}\right)^2 + \frac{\sigma_y}{3}\left[\left(\frac{\partial\varphi}{\partial\xi}\right)^2 + 4\left(\frac{\partial\varphi}{\partial\eta}\right)^2 - 4\left(\frac{\partial\varphi}{\partial\xi}\frac{\partial\varphi}{\partial\eta}\right)\right] + \sigma_z\left(\frac{\partial\varphi}{\partial\zeta}\right)^2\right\} d\xi\, d\eta\, d\zeta. \tag{4}$$

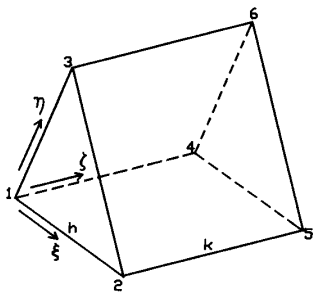

Fig. 4. Wedge-shaped volume element of the inhomogeneous model.

Derivatives in (4) were approximated by differences of potentials at the corner points of the wedges

$$\left(\frac{\partial\varphi}{\partial\xi}\right)^2 \simeq \left[(\varphi_1 - \varphi_2)^2 + (\varphi_4 - \varphi_5)^2\right]/2h^2 \tag{5a}$$

$$\left(\frac{\partial\varphi}{\partial\eta}\right)^2 \simeq \left[(\varphi_1 - \varphi_3)^2 + (\varphi_4 - \varphi_6)^2\right]/2h^2 \tag{5b}$$

$$\left(\frac{\partial\varphi}{\partial\zeta}\right)^2 \simeq \left[(\varphi_1 - \varphi_4)^2 + (\varphi_2 - \varphi_5)^2 + (\varphi_3 - \varphi_6)^2\right]/3k^2 \tag{5c}$$

$$\left(\frac{\partial\varphi\partial\varphi}{\partial\xi\partial\eta}\right) \simeq (\varphi_1 - \varphi_2 + \varphi_4 - \varphi_5) \cdot (\varphi_1 - \varphi_3 + \varphi_3 - \varphi_6)/4h^2. \tag{5d}$$

In combination with (4) an expression for P_w is obtained as a function of the potentials at the six corner points $\varphi_1 \cdots \varphi_6$: $P_w = P_w(\varphi_1 \cdots \varphi_6)$. Because the power dissipation P in the entire model is the sum of the power dissipations in all wedges, $P(\varphi) = \Sigma P_w(\varphi)$, an approximation $P(\underline{\varphi})$ of $P(\varphi)$ can be written as

$$P(\underline{\varphi}) = \underline{\varphi}^T M \underline{\varphi} \tag{6}$$

with $\underline{\varphi}$ a vector of the potentials at the grid points including points with a fixed potential (dirichlet points). $\underline{\varphi}^T$ is $\underline{\varphi}$ transposed. The elements of the system matrix M only depend on the discretization and on the model parameters. Minimizing power dissipation means minimizing $P(\underline{\varphi})$: $\partial P(\underline{\varphi})/\partial\tilde{\varphi}_k = 0$, with $\tilde{\varphi}_k$ the potential at any nonboundary gridpoint. This yields

$$M\underline{\tilde{\varphi}} + \underline{b} = \underline{0} \tag{7}$$

with $\underline{\tilde{\varphi}}$ the vector of the potentials at the nonboundary gridpoints and $\underline{b}$ a vector related to the dirichlet-points.

Equation (7) was solved iteratively (M is a sparse 61 240 × 61 240-matrix). Since a straightforward relaxation method is very time consuming a plane relaxation was used. The 3-D volume was divided into 2-D planes. During calculation of the potentials in plane k potentials of planes $k - 1$ and $k + 1$ were considered to be Dirichlet boundary conditions of plane k. After calculations in plane k were finished the same procedure was applied to plane $k + 1$ and so a (plane-wise) Gauss–Seidel iteration was performed. To calculate the potentials in a single plane a similar procedure was used. While potentials on horizontal line m in the plane were calculated, lines $m - 1$ and $m + 1$ were considered to be constant (line relaxation). After the calculation of line m was finished the procedure proceeded to line $m + 1$. The matrix M_{line} of the "line-equation" $M_{\text{line}}\underline{\varphi}_{\text{line}}$

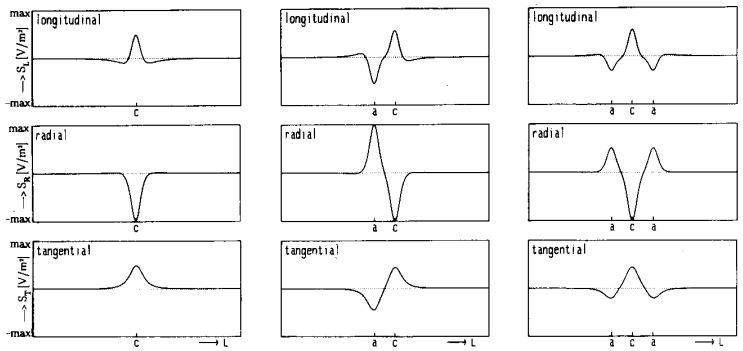

Fig. 5. Continuous longitudinal, radial and tangential activating functions at a line parallel to the L-axis at distance $d/2$ [dashed line in Fig. 2(b)] calculated in the homogeneous model for three different electrode configurations. Electrode positions are indicated by c (cathode) and a (anode); $\max = (1 + 5^{-5/2}) \cdot 4I/\pi\sigma d^3$. (a) monopolar (cathode), (b) bipolar (anode–cathode), (c) tripolar (anode–cathode–anode).

$= \underline{b}_{\text{line}}$ is tridiagonal, so the potentials at a line could be calculated very fast by using Gauss elimination.

Overrelaxation was performed on the full model (overrelaxation factor 1.7) until the following convergence-criterion was met [22]

$$\frac{\sum_{i=1}^{N} |\varphi_i^{j+1} - \varphi_i^j|}{\sum_{i=1}^{N} |\varphi_i^j|} < 0.001 \qquad (8)$$

with φ_i^j the potential at gridpoint i after j relaxations and N the number of gridpoints. One full model relaxation consists of eight relaxations in every plane. In order to investigate which parameters are important to the potential distribution in the spinal cord, sensitivity of the field potentials to conductivity of the model compartments was calculated as

$$\text{Sensitivity} = \frac{\sigma}{\varphi} \cdot \frac{\Delta\varphi}{\Delta\sigma} \qquad (9)$$

where $\Delta\sigma$ is the change in conductivity of the compartment and $\Delta\varphi$ the change in the average field potential in the dorsal columns due to this change in conductivity.

Results

Homogeneous Model

Results obtained from the homogeneous model are shown in Fig. 5. The continuous activating functions for fibers having a longitudinal, tangential or radial orientation were calculated at a longitudinal line at a distance $r = d/2$ from the L axis [the dashed line in Fig. 2(b)] where d is the distance between neighboring electrodes at the L axis. For a single cathode the peak value of the radial activating function is twice the peak value of the longitudinal and tangential ones and has opposite sign. This suggests that longitudinal and tangential fibers will be depolarized and radial fibers will be hyperpolarized. With anodal stimulation signs will be opposite. So in bipolar stimulation longitudinal fibers will be depolarized at a cathodal level and radial fibers at an anodal level.

TABLE III
Relative Values of the Maxima of the Continuous Activating Functions S_l, S_r, S_t in Three Orthogonal Directions in the Homogeneous Model at Lines at a Distance $d/2$ and 3 $d/2$ from the L-Axis [cf. Fig. 2(B)]

Configuration	Distance = $d/2$	Distance = 3 $d/2$
c	1:0.04:1	1:0.04:1
cc	1:0.05:1.25	1:0.06:1.39
a	1:9.88:0	1:9.83:0
aa	1:5.57:0	1:8.60:0
ac	1:1.81:0.81	1:1.50:0.5
aca	1:0.92:0.81	1:0.61:0.46
cac	1:3.32:0.69	1:3.15:0.31
acca	1:1.99:0.97	1:0.96:0.65
caac	1:1.76:0.88	1:2.38:0.38
acac	1:1.68:0.75	1:1.64:0.75

A comparison of the (positive) maxima of the activating functions in three orthogonal directions is shown in Table III. For each electrode configuration the maximum of the longitudinal activating function S_l was given the value 1. From this table it can be concluded that the electrode configuration with maximum directional selectivity for supposed depolarization of longitudinal fibers is anode–cathode–anode (aca). All configurations except c, cc, and cac have a dominating radial activating function. For selective stimulation of radial fibers one of the configurations a, aa, and cac will be a good choice. Configurations to depolarize tangential fibers are c and cc.

At a larger distance between electrodes and nerve fiber the activating functions of "monopoles" (a, aa, c, cc) decrease proportionally to $1/r^3$, while the decrease is even steeper in other configurations, especially in aca and cac.

Inhomogeneous Model

A computational and algorithmic test of the program for the inhomogeneous model was performed by Veltink [22] by comparing the numerical solutions of a cylindrical model, with the electrodes at the cylinder-axis, with the analytical solution. Both field potentials and activating functions at different positions

appeared to differ less than 5%. This is partly due to the difference in electrode dimensions: in the analytical model a point source was used and in the numerical one a hexagonal voltage source was used.

In the spinal cord model electrodes were located mediodorsally in the epidural space [Fig. 6(a), (c)]. Electrode length was 3 mm, diameter 1.5 mm and separation 6 mm, similar to the Medtronic Pisces Quad-electrode array. In Figs. 6 and 7 the isopotential lines are separated by 4% of the electrode potential and the smallest value of the isopotential lines shown is 4% of the electrode potential.

The number of relaxations needed, primarily depended on the electrode configuration. With a single electrode about 200 relaxation sweeps were needed to meet the convergence criterion and only about 100 in bipolar stimulation. This is due to the fact that the "bipolar solution" contains more high (spatial) frequencies and less low frequencies than the monopolar one.

In Fig. 6(a) the isopotential lines are shown in a transverse section at the midelectrode level. The lines in the spinal cord are not circular around the electrode as would be expected in a homogeneous medium. This is due to the shunting effect of the high conductivity of the csf-layer [Fig. 6(a) and (c)]. The isopotential lines in the csf layer are shown to be almost perpendicular to this layer and because the current density is perpendicular to the isopotential lines, most of the current is thus shunted by the csf layer.

Sensitivity of the field potential in the dorsal columns to variations in conductivity was determined according to equation (9). The highest value was found to be for the conductivity of the csf-layer and the white matter, with a sensitivity of 0.15 and 0.1 respectively in monopolar stimulation and 0.1 and 0.1 resp. in bipolar stimulation. This means that it is important to know these conductivities accurately. When the electrode is not in close contact with the cerebrospinal fluid then the sensitivity of the epidural fat is also important. In case the electrode-csf distance is 0.7 mm the sensitivity of the epidural fat is about 0.4.

Another important parameter is the width of the csf layer between the dorsal columns and the electrode(s). In the model an increase from 0.7 to 1.4 mm caused a decrease of 30% of the average field potential in the dorsal columns [Fig. 6(a), (b)]. At cervical levels this width may vary from about 5 mm to almost zero, depending on the set of the head.

An example of the effect of the inhomogeneity of the epidural space is shown in Fig. 7(a). At the right side of the electrode a compartment, having the dimensions of a small blood vessel ($1.2 \times 0.7 \times 60$ mm), was located aside the electrode. The conductivity was 0.008 $(\Omega\text{cm})^{-1}$, which is twenty times the conductivity of the surrounding epidural fat. As a result field potentials in the right part of the dorsal columns were about 4% higher than in the left part. If the electrode is separated from the csf by 0.7 mm this asymmetry is more than 10%.

Although in patients the electrode probe can be positioned well in the midsagittal plane, it often migrates in a lateral direction, and this will have an effect upon the field potential distribution in the spinal cord. The effect predicted for a lateral displacement of 1.5 mm is shown in Fig. 7(b). Field potentials at the right part of the dorsal columns are up to 15% higher than at corresponding positions in the left part.

It can thus be concluded that asymmetrical stimulation of the dorsal columns can be due to asymmetrical electrode location as well as inhomogeneous conductivity of the epidural space near the electrode(s), but the former cause is the most important one.

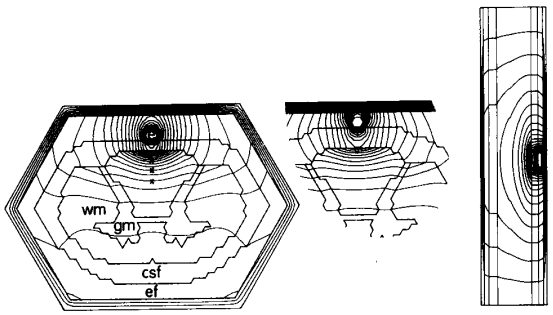

(a) (b) (c)

Fig. 6. Potential distributions in the inhomogeneous model, with monopolar anodal stimulation. (a) Isopotential lines in the transverse section at the mid-electrode level, wm = white matter, gm = gray matter, csf = cerebrospinal fluid, ef = epidural fat, e = electrode. The electrode is in the dorsal epidural space in the mid-sagittal plane. Isopotential lines are separated by 4% of the electrode potential. The smallest value is 4% of the electrode potential. Distance between dorsal boundary of the dorsal columns and the electrode is 0.7 mm. (b) Isopotential lines in the same transverse section as in (a) (dorsal column—electrode distance is 1.4 mm). (c) Isopotential lines in the midsagittal section.

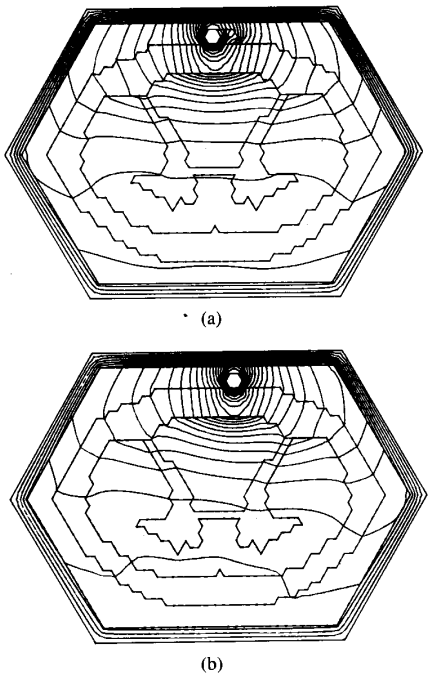

(a)

(b)

Fig. 7. Isopotential lines in the midelectrode level with anodal stimulation. The electrode is in the dorsal epidural space. (a) Small inhomogeneity at the right side of the midsagittal electrode. (b) Electrode at right side of the midsaggital plane. (For details see text.)

Longitudinal and radial activating functions along longitudinal lines in the dorsal columns at 0.7, 1.4 and 2.1 mm ["x" in Fig. 6(a)] away from the dorsal boundary are shown in Fig. 8(a) and (b) for monopolar and bipolar stimulation respectively. The isolines of the longitudinal activating function in this plane are shown in Fig. 8(c) (solid lines represent positive activating functions, dashed lines negative ones, lines near to the electrode were not plotted). Similar to the prediction by the homo-

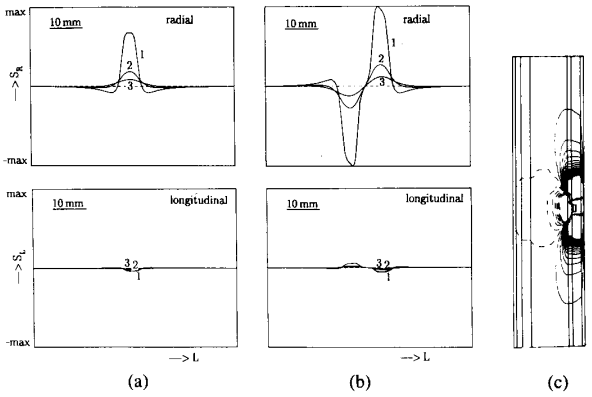

Fig. 8. Curves of longitudinal and radial activating functions at longitudinal lines at three midsagittal positions in the dorsal columns at 1) 0.7, 2) 1.4, and 3) 2.1 mm away from the dorsal boundary as indicated by "x" in Fig. 6(a). (a) Anodal monopolar stimulation. (b) Bipolar stimulation (anode–cathode). (c) Isolines of the longitudinal monopolar activating function in the midsagittal section. Solid lines are positive, dashed lines negative. Lines near the electrode are not plotted.

geneous model radial and longitudinal activating functions have opposite signs. However, in the inhomogeneous model the peak value of the radial activating function is more than ten times the longitudinal one at monopolar stimulation (two times in the homogeneous medium). In the bipolar case the ratio of the peak values of the radial and longitudinal activating functions is somewhat higher than in the monopolar case. This difference between the homogeneous and inhomogeneous model is mainly due to spreading of the current in longitudinal and lateral direction caused by the cerebrospinal fluid. The potential gradients in the dorsal columns in these directions are reduced as compared to the gradients in dorsoventral direction.

Discussion

The significance of the present study is not limited to the analysis of electrode configurations already in use, thus helping to gain insight into the mechanisms of spinal cord stimulation. A major goal is also to design alternative electrode configurations for the selective stimulation of neural pathways in the spinal cord.

Validation of the model is very difficult. The best way to do it, would be to measure field potentials in the spinal cord in situ as reported by Swiontek *et al.* [5] who placed the stimulating electrodes at the surface of the spinal cord. As we have shown, the csf layer has a major influence on the potential distribution in the spinal cord. The significance of the study by Swiontek is thus limited with respect to epidural spinal cord stimulation *in situ*.

The shape of the isopotential lines in the spinal cord in the transverse as well as in the midsagittal section is similar to those of Coburn and Sin in their 3-D model, as is the slight distortion caused by the gray matter.

The variability of the width of the csf-layer imposes serious limitations on the predictability of the effects of epidural spinal cord stimulation and on the possibility of creating a stable stimulation of specific spinal pathways. The influence of varying the width of the csf layer on the field potentials in the dorsal columns is confirmed by clinical observations of a patient with cervical epidural stimulating electrodes. When the head was bend forward the threshold amplitude of the stimulator to evoke parethesia increased by about 20%. In our model an increase of the width of the csf layer by 100% gave a decrease in average field potential and activating functions in the dorsal columns of about 30%. So the effects of the varying width of the csf layer, as predicted by the model, are at least of the same order of magnitude as was observed in this patient.

Potentials, due to spinal cord stimulaton, that were measured on the body surface of a patient appeared to be almost zero. Therefore the Dirichlet boundary condition (3b) that was used at the model surface instead of the natural Neumann condition (current density perpendicular to the body surface is zero) seems a good approximation of the natural boundary condition and diminishes computation time. The validity of the low conductivity border, representing the surrounding tissues, might be investigated by modeling these tissues as a much larger compartment. However this would increase the number of grid points enormously. When varying the conductivity of this compartment field potentials in the dorsal columns did not change significantly; the sensitivity of this compartment was less than 1%.

In general the kind of convergence criterion that was used (8) is not very reliable because relaxation methods often converge very slowly to their ultimate solution. The local character of these methods causes low spatial frequency solutions to be obtained slowly. In the method presented here this is less important because relaxation was performed in one dimension each time. When increasing the number of iterations by a factor five in one simulation the solution changed by less than 1%.

The next step in modeling spinal cord stimulation is to investigate the effect of the imposed potential distribution on nerve fibers. Fiber diameter and electrode-fiber distance [12], [22] are important parameters in selective nerve stimulation. In the homogeneous model it was shown that fibers with different orientations may respond differently to a given electrode configuration. As a first approximation of the influence of the potential field on nerve fibers we used the activating function [10]. The activating function determines the initial change of membrane potential. (For a passive unmyelinated fiber the well known partial differential equation is: $\lambda^2(\partial^2V/\partial^2x) - \tau(\partial V/\partial t) - V = -\lambda^2 S$ where S is the activating function, V is the difference between the actual membrane potential and the membrane resting potential, τ is the membrane time constant and λ is the length constant. When the fiber is at rest and therefore $V = 0$ and $\partial^2V/\partial^2x = 0$, then at the onset of the stimulating pulse $\partial V/\partial t = \lambda^2 S/\tau$ and therefore initially the membrane potential of a long fiber will be entirely determined by the activating function. The same conclusion holds for a myelinated fiber). The activating function is only meaningful for long fibers because for short fibers the boundary conditions of the differential equation are of major importance. The collateral fibers in the dorsal columns might be too short for using a simple straight fiber activating function. To obtain a more realistic quantitative description, a nonlinear membrane model will be used for the calculation of the effect of stimulation on the nerve membrane.

References

[1] C. N. Shealy, J. T. Mortimer, and J. B. Reswick, "Electrical inhibition of pain by stimulation of the dorsal columns: Preliminary clinical report," *Anesthesia analgesia—Current Researches*, vol. 46, pp. 489–491, 1967.

[2] R. Melzack and P. D. Wall, "Pain mechanisms: A new theory," *Science*, vol. 150, pp. 971–979, 1965.

[3] P. D. Wall, "The gate-control theory of pain mechanisms. A reexamination and restatement," *Brain*, vol. 101, pp. 1-18, 1978.
[4] J. Gybels and D. van Roost, "Spinal cord stimulation for the modification of dystonic and hyperkinetic conditions: A critical review," in *Recent Achievements in Restorative Neurology*; Book 1: Upper motor neuron functions and dysfunctions. Basel, Karger 1985, pp. 56-70.
[5] T. J. Swiontek, A. Sances, S. J. Larson, J. J. Ackmann, J. F. Cusick, G. A. Meyer, and E. A. Millar, "Spinal cord implant studies," *IEEE Trans. Biomed. Eng.*, vol. BME-23, pp. 307-312, 1976.
[6] J. B. Rusinko, C. F. Walker, and N. G. Sepulvedo, "Finite element modeling of potentials within the human thoracic spinal cord due to applied electrical stimulation," *Frontiers of engineering in health care, vol. 3*, in *Proc. IEEE-EMBS Conf.*, Houston, TX, 1981, pp. 76-81.
[7] B. Coburn, "Electrical stimulation of the spinal cord: Two-dimensional finite element analysis with particular reference to epidural electrodes," *Med. Biol. Eng. Comp.*, vol. 18, pp. 573-584, 1980.
[8] W. K. Sin and B. Coburn, "Electrical stimulation of the spinal cord: A further analysis relating to anatomical factors and tissue properties," *Med. Biol. Eng. Comp.*, vol. 21, pp. 264-269, 1983.
[9] B. Coburn, W. K. Sin, "A theoretical study of epidural electrical stimulation of the spinal cord—Part 1: Finite element analysis of stimulus fields," *IEEE Trans. Biomed. Eng.*, vol. BME-32, pp. 971-977, 1985.
[10] F. Rattay, "Analysis of models for external stimulation of axons," *IEEE Trans. Biomed. Eng.*, vol. BME-33, pp. 974-977, 1986.
[11] D. R. McNeal, "Analysis of a model for excitation of myelinated nerve," *IEEE Trans. Biomed. Eng.*, vol. BME-23, pp. 329-337, 1976.
[12] F. Rattay, "Ways to approximate current-distance relations for electrically stimulated fibers," *J. Theoretical Biol.*, vol. 125, pp. 339-349, 1987.
[13] R. A. Davidoff, Ed., *Handbook of the Spinal Cord, Vol. 2 and 3: Anatomy and Physiology.* New York, Marcel Dekker, 1983.
[14] L. A. Geddes and L. E. Baker, "The specific resistance of biological material—A compendium of data for the biomedical engineer and physiologist," *Med. Biol. Eng.*, vol. 5, pp. 271-293, 1967.
[15] C. H. Elliott, "Cross-sectional diameters and areas of the human spinal cord," *Anat. Rec.*, vol. 93, pp. 287-293, 1945.
[16] L. Nordqvist, "The sagittal diameter of the spinal cord and subarachnoid space in different age groups: A roentgenographic post-mortem study," *Acta Radiologica*, suppl. 227, pp. 1-96, 1964.
[17] L. Penning, J. T. Wilmink, H. H. van Woerden, and E. Knol, "CT myelographic findings in degenerative disorders of the cervical spine: Clinical significance," *Amer. J. Radiol.*, vol. 146, pp. 793-801, 1986.
[18] H. O. M. Thijssen, A. Keyser, M. W. M. Horstink, and E. Meijer, "Morphology of the cervical spinal cord on computed tomography," *Neuroradiol.*, vol. 18, pp. 57-62, 1979.
[19] I. O. Skalpe and O. Sortland, "Cervical myelography with metrasimide (amipaque)," *Neuroradiol.*, vol. 16, pp. 275-278, 1978.
[20] T. C. Pilkington, M. N. Morrow, and P. C. Stanley, "A comparison of finite element and integral formulations for the calculation of electrocardiographic potentials," *IEEE Trans. Biomed. Eng.*, vol. BME-32, pp. 166-173, 1985.
[21] J. P. Aubin, "Approximation of elliptic boundary-value problems," *Pure and Applied Mathematics Vol. XXVI.* New York: Wiley, 1972.
[22] P. H. Veltink, B. K. van Veen, J. J. Struijk, J. Holsheimer, and H. B. K. Boom, "A modeling study of fascicle selective nerve stimulation," *IEEE Trans. Biomed. Eng.*, vol. BME-36, pp. 683-692, 1989.

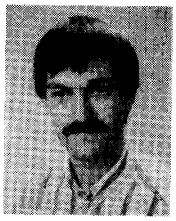

Johannes J. Struijk (S'89) was born in Rijssen, The Netherlands, in 1963. He received the M.Sc. degree in electrical and biomedical engineering from the University of Twente, Twente, The Netherlands, where he currently is working as a Ph.D. student at the Biomedical Engineering Division of the Department of Electrical Engineering. His research interests are related to spinal cord stimulation and involve volume conduction and neural modeling.

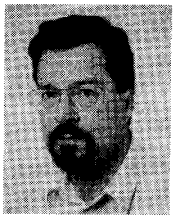

Jan Holsheimer was born in Enschede, The Netherlands, in 1941. He received the M.Sc. degree in biology and biophysics from the University of Groningen, The Netherlands, in 1965 and the Ph.D. degree in biomedical engineering from the University of Twente, Enschede, in 1982.

In 1965 he joined the Biomedical Engineering Division, Department of Electrical Engineering, University of Twente. His research interests are volume conduction and the analysis of field potentials in the brain and electrical stimulation of nervous tissue.

Benno K. van Veen was born in Vaassen, The Netherlands, in 1963. He received the M.Sc. degree in electrical engineering from the University of Twente, Enschede, The Netherlands, in 1988.

Since 1988 he has been working towards the Ph.D. degree at the Biomedical Engineering Division of the Department of Electrical Engineering at the University of Twente. His current research activities involve the electrical activity and volume conduction in skeletal muscle.

Herman B. K. Boom (M'89) was trained as a Medical Physicist at the University Utrecht, The Netherlands, where he received the Ph.D. degree in 1971.

He joined the Departments of Medical Physics and Medical Physiology where he was engaged in research in the field of cardiac mechanics and taught physiology and biophysics. Since 1976 he has held the Chair of Medical Electronics in the Department of Electrical Engineering, University of Twente, The Netherlands. His research interests are cardiovascular system dynamics, bioelectricity, and rehabilitation technology.